Comparison of Volatiles Evolving from Selected Highland and Mare Lunar Regolith Simulants During Vacuum Sintering

Petkov, Mihail
Wilkerson, Ryan Patrick
Voecks, Gerald E.
Rickman, Doug
Edmunson, Jennifer
Effinger, Michael R.

To be published in: Planetary and Space Science

DOI to publisher's version: 10.1016/j.pss.2024.105982

Comparison of Volatiles Evolving from Selected Highland and Mare Lunar Regolith Simulants During Vacuum Sintering

Mihail P. Petkov, Ryan P. Wilkerson, Gerald E. Voecks, Douglas L. Rickman, Jennifer E. Edmunson, Michael R. Effinger

PII: S0032-0633(24)00146-6

DOI: https://doi.org/10.1016/j.pss.2024.105982

Reference: PSS 105982

To appear in: *Planetary and Space Science*

Received Date: 17 April 2024

Revised Date: 13 August 2024

Accepted Date: 30 September 2024

Please cite this article as: Petkov, M.P., Wilkerson, R.P., Voecks, G.E., Rickman, D.L., Edmunson, J.E., Effinger, M.R., Comparison of Volatiles Evolving from Selected Highland and Mare Lunar Regolith Simulants During Vacuum Sintering, *Planetary and Space Science*, https://doi.org/10.1016/j.pss.2024.105982.

Comparison of Volatiles Evolving from Selected Highland and Mare Lunar Regolith Simulants During Vacuum Sintering

Mihail P. Petkov[1*], Ryan P. Wilkerson[2], Gerald E. Voecks[3], Douglas L. Rickman[4], Jennifer E. Edmunson[5], and Michael R. Effinger[5]

[1]*SuprAEther LLC, La Crescenta, California 91214, U.S.A.*

[2]*Sigma-1: Fabrication Manufacturing Science, Los Alamos National Laboratory, Los Alamos, NM, 87545, U.S.A.*

[3]*NASA Jet Propulsion Laboratory, California Institute of Technology, Pasadena, California 91109, U.S.A.*

[4]*Jacobs Engineering, Inc., Huntsville, AL 35812, U.S.A.*

[5]*NASA Marshall Space Flight Center, Huntsville, AL 35812, U.S.A.*

*Corresponding author: mppetkov@supraether.com

ORCID: 0000-0002-2739-6928

Highlights:

- Heated lunar regolith simulants generate large gas loads, forming a complex mixture of volatiles that promotes a wide range of reactions.
- Volatiles, comprising the self-generated environment, were attributed to specific sources using mineralogical knowledge of the simulants.
- Information, pertaining to the decomposition of non-lunar phases, can guide methodologies for enhancing the simulants fidelity.

Abstract

Volatiles evolving from JSC-1A, NU-LHT-4M and CSM-LHT-1G lunar regolith simulants during *in vacuo* thermal processing were analyzed using mass spectrometry as a function of temperature. Two high-fidelity simulants, JSC-1A (mare) and NU-LHT-4M (highland), were compared to a newly developed CSM-LHT-1G highland simulant, modified to closely match lunar geochemistry. Large autogenous gas loads were observed for all investigated materials. Mineralogical knowledge was used to identify and attribute individual volatile species to reacting, transforming, or decomposing constituents (hydrates, carbonates, sulfates, sulfides, clays, etc.) of the respective regolith simulant in the self-generated gas environment. Cumulative mass losses for individual simulant components as a function of temperature were quantified using mass spectrometry in conjunction with thermogravimetric analysis. Investigation of the four components of CSM-LHT-1G – anorthosite, basalt, augite, and glass – aided the attribution of volatile species to specific compounds and their respective sources. The results showed significant decomposition of non-lunar phases present in the man-made regolith simulants below the typical glass crystallization temperatures, which paves the way to devising methods for enhancing the fidelity of the simulants. High gas loads and corrosive gases (HF and HCl) were recognized as potential hazards, pertaining to the development of large testbed facilities.

1 Introduction

The establishment of a permanent human presence on the Moon and Mars is envisioned as the embodiment of the next stage of space exploration by the National Aeronautics and Space Administration (NASA) and other space agencies. NASA's Artemis program (NASA, 2020) presents the roadmap for achieving these goals, working in cooperation with other space agencies and private corporations. The Artemis program seeks the development of a range of technologies with emphasis on in-situ resource utilization (ISRU). ISRU is an indispensable approach for human exploration. It reduces terrestrial dependence, decreases mission costs and risk, enables faster progress, supports complex operations, and facilitates continuous human presence.

ISRU includes direct processing of lunar regolith for construction through thermal, microwave and laser sintering (Taylor and Meek, 2005; Krishna Balla et al., 2012; Farries et al., 2021; Whittington and Parsapoor, 2022; Suhaizan et al., 2023) and additive manufacturing (Cesaretti et al., 2014; Howe et al., 2014; Goulas and Friel, 2016; Isachenkov et al., 2021; Altun et al., 2021) and extends to a broad range of materials benefaction – oxygen, water, fuels, metals, silicon, etc., (Taylor and Carrier, 1993; Allen et al., 1996; Rasera et al., 2020; Schlüter and Cowley, 2020; Guerrero-Gonzalez and Zabel, 2023). The advancement of relevant technologies necessitates testing and validation with lunar regolith, only limited amounts of which exist from the Apollo missions. Large-scale operations would undeniably require man-made regolith simulants with sufficient fidelity for use as proxies. The simulants must closely represent the composition, mineralogy, particle size and shape, and density of the lunar regolith at a given lunar site. Fabrication of such materials had been undertaken by both government agencies and private institutions in several countries, resulting in a wide variety of simulants (Toklu and Akpinar, 2022; NASA, 2024). However, inherent major mineralogical differences, generated by rock formation and weathering processes on Earth, render the lunar regolith distinctly different from any engineered simulant (Heiken et al., 1991). Even over short geological times (thousands

of years), some of the original phases in igneous rocks used for simulant fabrication have been converted to altered stable phases, such as carbonates, sulfates, hydrated oxides, clays, etc., which are not present in lunar mineralogy. Conversely, nanophase Fe^0-rich agglutinates, made by hypervelocity micrometeorite impacts on the Moon, have no natural Earth equivalents. Production of suitable analogs in large quantities is an arduous and complex endeavor and has been a limiting factor in the production of high quantities of more lunar-like simulants. However, the fidelity of any lunar regolith simulant is not a comprehensive characteristic but must be assessed in the context of the intended application.

Replicating lunar characteristics is essential for the characterization and testing of lunar regolith simulants for ISRU applications to avoid undesirable effects. These include surface moisture from ambient air affecting triboelectric charging (Anderson et al., 2009), powder flow and particle packing, high-temperature decomposition of non-lunar components generating inherent gaseous atmosphere (Petkov and Voecks, 2023), hydrocarbons from thermal decomposition of organic matter facilitating thermochemical sulfate reactions (Zhang et al, 2007), etc. While lunar vacuum (~10^{-12} mbar) may be difficult or cost-prohibitive to replicate in a laboratory, the experimental conditions must be assessed in the context of self-generated pressure within a simulant sample to minimize Earth-inherent experimental biases. High-vacuum (<10^{-6} mbar) (Petkov & Voecks, 2023) and/or high conductance systems (Cardiff et al, 2007) can often prove adequate.

Identification and quantification of volatile species, evolving during heating of lunar regolith simulant materials in vacuum to sintering and melting temperatures, provide valuable information on inherent non-lunar components (Petkov & Voecks, 2023). This allows for a direct comparison of different materials, or provides the fundamental knowledge needed to devise a thermal process, intended to reduce or remove undesirable components. Using this approach, Wilkerson et al. (2023) optimized the thermal treatment of JSC-1A to reduce its non-lunar phases without significant impact on its figure of merit, thereby generally enhancing the simulant's fidelity.

The first part of the present work reports results from the comparison of three simulant materials – JSC-1A (mare), NU-LHT-4M (highland), and CSM-LHT-1G (highland). High-dynamic-range mass spectrometry (MS) was utilized for the characterization of volatile signatures arising from the decomposition of non-lunar components (carbonates, sulfates, etc.), which were then identified using mineralogical information and quantified using thermogravimetric analysis (TGA) in conjunction with MS. In the second part, the MS characteristics of the CSM-LHT-1G simulant is compared to a compositional spectrum comprised of its four primary constituents (anorthosite, basalt, augite, and glass), measured individually and weighted with the respective mass fraction in the composite. This aided the identification of the source of individual non-lunar phases in CSM-LHT-1G, linked to the respective component. CSM-LHT-1G was the only compound simulant for which all of the individual components were available separately, aiding such investigation.

2 Materials and Methods

2.1 Simulant Materials

This comparison includes three different regolith simulants – JSC-1A, NU-LHT-4M, and CSM-LHT-1G. Like all lunar simulants, these are made from igneous rocks, wherein the

primary, *i.e.*, original, mineralogy is usefully close to lunar mineralogy. JSC-1A is a lunar mare simulant, derived from a basaltic volcanic ash from Merriam Crater near Flagstaff, Arizona, USA. It was made for Orbital Technologies Corporation (Gustafson et al., 2006) under a NASA contract as a replenishment of the original JSC-1 stockpile. JSC-1A was intended for wide distribution and is the most thoroughly investigated and characterized of the lunar simulants. NU-LHT-4M is a lunar highlands simulant, made by the United States Geological Survey in collaboration with NASA. Its design is a close duplicate of NU-LHT-2M (Stoeser et al, 2010). Quantities of -2M produced, ~500 kg, were within the allowances of the available high-quality glass. Due to the shortage of NU-LHT-2M/4M, a more accessible highlands simulant was needed until a higher fidelity simulant becomes available. To this end, CSM-LHT-1G was devised by NASA Marshall Space Flight Center on the basis of the Colorado School of Mines highland simulant CSM-LHT-1, which comprises 70 wt.% GreenSpar anorthosite and 30 wt.% Merriam Crater basalt (NASA, 2024). The CSM-LHT-1 composition was modified to closely match the lunar geochemistry per Lemelin et al. (2015). This was achieved with the addition of commercial augite from Ward's Science, VWR International (VWR), and glass produced by Washington Mills (WM) intended for the development of NUW-LHT-5M. The augite, obtained from surface exposure of syenite pegmatite, was partly weathered and contained minor impurities of microcline, fluorite, and scapolite. The resulting proportions of the CSM-LHT-1G components were 55.2 wt.% GreenSpar anorthosite, 23.6 wt.% Merriam Crater basalt, 6.0 wt.% VWR augite, and 15.2 wt.% WM glass.

Individual samples of the four CSM-LHT-1G constituents, each weighing 10.0 g, were also characterized separately using mass spectrometry. To compare to the CSM-LHT-1G composite, a combination spectrum was then generated as a linear superposition, in which each component contribution was weighed with the respective mass fraction in the simulant. Such analysis is in line with the fundamental principals of quantitative mass spectral analysis, established by Washburn et al. (1943).

2.2 Vacuum Furnace Sintering

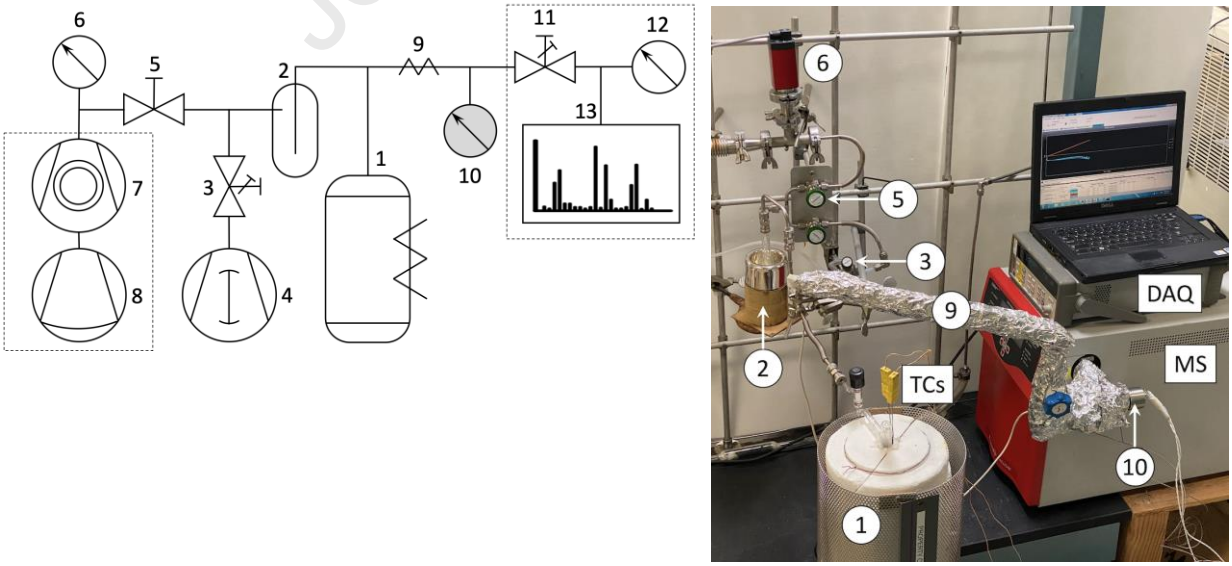

Figure 1. Schematic drawing (left) and annotated image of the experimental apparatus (right). For detailed description see Petkov & Voecks (2023), published in Ceramics

International, Copyright Elsevier 2023. Here, the relevant elements are: 1 – furnace; 2 – cold trap; 9 – heated vacuum line, 10 – micro-Pirani gauge (main pressure sensor); and mass spectrometer (including 11, 12 and 13).

Experiments were carried out in a high-vacuum system (**Figure 1**) with a base pressure of $<10^{-6}$ mbar (without sample), equipped with a mass spectrometer, and designed to handle large gas loads evolving from heated regolith samples (Petkov & Voecks, 2023). Regolith samples in powder form were sealed in quartz vessels and placed in a tube furnace with a maximum temperature of 1300ºC. The thermal profile was identical for all measurements: 1ºC/min up to 125ºC, then 2.5ºC/min to temperatures exceeding the respective material melting temperatures. The typical vacuum level at the start of an experiment was $\sim 2\times10^{-6}$ mbar; however, peak pressures at the sample, caused by high gas loads from decomposition products, ranged from ~0.06 mbar to ~0.3 mbar. The split-flow system was designed to provide high pumping capacity for large gas loads, generated by the regolith, while simultaneously delivering adequate gas flow to a residual gas analyzer (RGA, based on a quadrupole mass analyzer) for maximizing its efficiency for volatiles identification and quantification. Measurements of the gas flow fractions through the system were done in system configurations similar to these reported in the above reference with atmospheric air flowing through a pinched capillary tube calibration standard (Vacuum Technology Inc., Oak Ridge, TN, USA) with a rate of $(9.3\pm0.5)\times10^{-8}$ standard l/s air (temperature corrected value). Absolute ambient pressure measurements were taken with a Taber 254-SA pressure transducer (Taber Industries, North Tonawanda, NY, USA) with ±2 mbar (0.12% full-scale) accuracy. The resulting flow rate estimates were 62±3% for JSC-1A and 29±1.5% for all other experiments, including NU-LHT-4M, CSM-LHT-1G, and the four components of the latter. These values are in a good agreement with the previously reported ones using dimensional calculations (Petkov & Voecks, 2023).

The achieved RGA dynamic range exceeded five orders of magnitude, ensuring sensitivity to minor and trace compounds in the simulants. The reported pressure values in our work are given as pressures at the sample, not at the sensor location. This important distinction from other published reports offers a closer representation of self-generated atmospheres by the regolith simulants (or actual lunar regolith). Calibration of the pressure at the sample and other system performance and characterization aspects were discussed elsewhere (Petkov & Voecks, 2023).

2.3 Thermogravimetric Analysis

Mass loss and volatiles identification was carried out with a SETSYS Evolution (Setaram, Lyon, France) TGA instrument with integrated MS capability from a quantitative gas analysis quadropole mass spectrometer (Hidden Inc, Peterborough NH, USA). The MS had lower dynamic range than the present system and, thereby, lower sensitivity to trace volatile signatures. Although not reported here, all MS results were in good agreement with the data presented in this work; this was used as independent verification of the outgassing products from the dominant sources. Here we report the TGA results obtained under vacuum conditions ($<1\text{x}10^{-4}$ mbar), provided by a HiCube 80 Eco turbopump vacuum system (Pfeiffer Vacuum Inc., Nashua, NH, USA). Large volume TGA crucibles allowed for specimen sizes of 1500 mg, which minimized sample-to-sample variations and allowed for collecting strong outgassing MS

signals. The TGA thermal profiles for each sample replicated these used in the furnace sintering experiments.

3 Results and Discussion – Part A: Comparison of JSC-1A, NU-LHT-4M and CSM-LHT-1G Lunar Regolith Simulants

3.1 Mineralogical Background

The major non-lunar components in man-made lunar simulants can be either primary or secondary minerals. Primary minerals, gases, and volcanic glass if present, classed as primary components, were created when the original rock formed from the magma; secondary minerals were formed later. Secondary minerals come from either weathering on Earth's surface, metamorphism, or hydrothermal alteration. The exact mineralogy of a simulant records the geologic history of the feedstocks used to make the simulant. Minerals are also classified by their elements. The combination of geologic history and the elements put significant constraints on the interpretation the data presented herein.

Most volatile evolution requires either a change in crystallization, rupture of pores containing trapped liquid or gas, or melting or sublimation of constituents in the simulant. The primary minerals used in lunar simulants are, with minor exceptions, not affected significantly by temperatures below ~750°C. Relevant glass, if present, will begin to crystalize near that temperature, potentially allowing trapped primary gases, especially sulfur compounds, to escape. Weakening of particles and resultant volatile evolution can occur for several reasons, especially in particles that are heterogenous, and the expected temperature range is very problematic to predict. Melting of the relevant minerals generally will start in the 1100°C to 1250°C range in the presence of a glass, or at temperatures as much as 300°C hotter in simulants that are essentially mono-mineralic and truly devoid of molecules such as H_2O. It is useful to note that temperatures of gas evolution from minerals generally correlates with geologic temperatures of formation.

The volatile evolution of secondary minerals varies substantially in temperature and commonly occurs at temperatures well below 1000°C. Each mineral has its own specific and frequently broad range of temperatures over which it will decompose, yielding gas.

Geologists also classify abundance of each phase in the composition in a simulant using the informal terms major, minor, or trace. Minor phases have an abundance between approximately 5 to 0.5 wt%, while major phases are more abundant and trace phases have less. This informal boundary also roughly corresponds to the difficulty of finding and identifying a mineral in the simulant or the feedstocks used to make the simulant. Minor minerals are generally beyond the reach of x-ray diffraction (XRD), and trace minerals require knowledgeable searching using appropriate techniques. As a practical matter, the exact identity of the trace and even some of the minor minerals, which can contribute substantially to gas evolution from a simulant during heating, is frequently unknown, and geologic reasoning must be used to suspect their presence.

Because of the preceding, relating observed volatile evolution to specific causes within a simulant is problematic. For attribution to a cause, information is needed on (1) the known mineralogy, (2) information about the multiple geologic environments the feedstocks have seen, (3) decomposition temperatures of candidate minerals, (4) the abundance of the root elements or radicals in the candidate minerals, and (5) the mass balances of candidate minerals versus the

observed gas evolution. Given that exact mineralogy of the simulants is at best known only for the major minerals and some minor (and rarely some trace) minerals, and the exact compositions of such candidate minerals as the carbonates are not known, the absolute inversion of the gas measurement to mineralogy is not possible. Therefore, reasoned guesses must be made.

3.2 Specific Minerals and Groups

General guidance is derived from knowledge of the source rock's exact geologic history. This knowledge strongly constrains which primary and secondary minerals are reasonable to consider. It also constrains such factors as potential gases released from primary glasses, and the fluid compositions of ubiquitous fluid inclusions. Another factor is the certain presence of minor and trace minerals. These phases, commonly ignored when discussing simulants, can be notable contributors to specific gas evolution. Whereas the major minerals in a feedstock rock may be acceptably lunar-like, the minor and trace minerals commonly are not. Analogous to rocks, minerals can have minor or trace elements. And finally, the integrity of a mineral's lattice becomes a factor. A poorly crystallized mineral derived from weathering can act different than the well crystalized form.

Minor, trace minerals, the state of crystallization, and particle sizes are generally not well known in feedstocks used to make simulants. For most users these phases generally do not matter. Also, they are not practical to detect using XRD, scanning electron microscopy (SEM) and other common techniques. Processes designed specifically to even detect them are required. Therefore, geologic reasoning is used to supplement what is measured.

Water, *sensu lato*, exists in minerals a number of ways. For instance, it can be an essential part of the lattice, which is the case with gypsum, $CaSO_4 \cdot 2H_2O$; gypsum is found in all simulants derived from the Merriam Crater feedstocks. Both amphibole group minerals, such as hornblende, and micas, such as biotite, contain OH^- radicals and are found in both NU-LHT-4M and CSM-LHT-1G. Various members of the clay family, which may contain both H_2O and OH^-, are known in Merriam Crater materials, NU-LHT-4M, and the anorthosite used to make CSM-LHT-1G. The specific clay(s) in each are probably different, each mineral having its own temperature range for decomposition and evolvable water mass.

Water, *sensu stricto*, also is found at grain boundaries and inside crystals as fluid inclusions. Fluid inclusions are sealed vesicles within a crystal which contain some of the fluid from which the crystal grew. Especially in the igneous rocks used to make simulants, these packets of fluid were trapped at high temperature, high pressure, and highly concentrated solutions. When the crystal lattice fails during heating in a vacuum, the supercritically heated H_2O (>374ºC) flashes to gas and other elements can be released.

Clays are of particular interest for several reasons. Their lattice structures (refer to Section 5 in Krūmiņš et al., 2022) allow incorporation of multiple constituents, some of which are easily liberated on heating. While H_2O is the normally expected gas to be evolved from a clay, other phases, i.e. OH^-, F^-, Cl^-, or elements, may also be present, again dependent on the geologic history of the feedstocks. Clays can also evolve volatiles over a wide range of temperatures and the evolution can appear to be continuous over a wide range. Finally, multiple clays can be present in a single source, each clay having its own thermal evolution behavior.

Related to clays are several other mineral groups, such as epidotes, zoisite, and chlorite. These are known to be in the hydrothermal-magmatic ore system at Stillwater Montana that

provides the crystalline feedstocks used to make NU-LHT-4M (Boudreau, 2016). Such minerals can also liberate volatiles when heated.

Carbonates, minerals containing the CO_3^{2-} ion, are characteristic in all three secondary geologic environments, both at low and high temperature. The most common carbonate is calcite, $CaCO_3$. In addition to Ca carbonate, there are also (Mg,Ca) and Fe carbonates in the simulants reported here. Carbonates are explicitly known in the Stillwater Complex (Aird and Boudreau, 2013) and in the Qaqortorsuaq anorthosite southwest of Kangerlussuaq, Greenland which is used in making CSM-LHT-1G (internal NASA data, 2019). Based on known geology, carbonates are certainly present in the Merriam Crater material used to make JSC-1A. In JSC-1A the calcite occurs, at least in part, in the form of caliche. Caliche can have very small crystal sizes and the calcite is mixed with a range of other minerals, such as sulfates, *i.e.*, gypsum.

Sulfur exists in the simulants as primary sulfide minerals, as an admixed constituent inside volcanic glass, and in the semi-arid weathering environment of Merriam Crater, as sulfates. Troilite, FeS, the sulfide identified in lunar samples, is not found naturally on Earth. Its Earth analog is pyrite, FeS_2, which is far the dominant primary form of sulfide in all simulants. Other sulfides are also known in the three simulants. For example, the most thoroughly studied in this respect is the source rock used to make NU-LHT-4M (Aird et al., 2017). The rock is from a sulfide assemblage carrying platinum. Some of the sulfides known to be present include pyrrhotite, copper sulfides and zinc sulfide. However, the sum of their masses in the simulant are expected to be much less than 0.5 wt%. Secondary sulfur phases are present in the Merriam Crater source material, due to weathering processes operating on primary pyrite. Pyrite would be a normally expected trace or minor mineral in the Greenland source for CSM-LHT-1G, although the necessary work to identify it has not been done. The secondary sulfates in Merriam Crater material include gypsum and basanite, but others, such as iron-bearing phases are highly likely.

There are multiple primary minerals in these simulants that are very likely to carry F and Cl. Micas, like biotite and muscovite, are known in the feedstocks of NU-LHT-4M and CSM-LHT-1G. Based on geology, JSC-1A may also have at least one of the minerals in this class. The apatite group is known in NU-LHT-4M and is expected in both JSC-1A and CSM-LHT-1G. Samples of CSM-LHT-1G, Merriam Crater basalt (JSC-1A), GreenSpar anorthosite, and augite were analyzed for water-soluble F and Cl content. Detected trace values of note were 0.36-0.38 wt.% F and 0.06-0.07 wt.% Cl in the augite, and 0.06 wt.% Cl in the basalt; all other measurements were below the detection limits (<0.1 wt.% for F and <0.02 wt.% for Cl).

Our data herein have very high sensitivities. As such the volumes of potential source minerals needed to explain the measurements are relatively small, certainly in the minor as well as the trace abundance ranges. But any one of our measurements might be attributed to multiple sources. With the knowledge that minerals of primary origin are largely not involved in gas evolution below at least 750°C, and probably 1000°C, it is practical to estimate the total amount of secondary minerals in a simulant. This is done using a Loss on Ignition (LOI) test, in which a measured aliquot of simulant is heated in a furnace, e.g., 1000°C, then reweighed. The available information indicates the LOI for all three simulants is $\lesssim$1 wt%, but the current data must be considered minimum numbers as these simulants gain weight when T$\gtrsim$400°C through oxidation supplied by air, even as volatiles are released (Street et al., 2010). On the other hand, the low LOI and our TGA mass loss measurements align quite well with the fact the composition of these simulants is strongly dominated by the desired primary minerals, which are reasonably lunar-like.

3.3 Autogenous Pressure Environment

Simulants comparison was carried out with samples of similar weights: JSC-1A (23.1 g), NU-LHT-4M (23.7 g), and CSM-LHT-1G (23.4 g). Each material was sealed in a quartz tube reactor with a bulb-shaped bottom, intended to optimize the RGA time response to changes that may experience delays due to gas transport through the sample bulk. The pressure-temperature profiles of the three materials (**Figure 2**) were adjusted for total pressure, accounting for the different flow rate fractions in the split-flow system. Each material was heated to a temperature above its melting point. The occurrence of a melt was deduced from the onset of the pressure bursts, which were attributed to decrepitation events – sudden release of gas from vesicles, termed "fluid inclusions", formed when igneous fluids were trapped at high pressure in minerals at the time of their formation. The decrepitation onset temperatures were 1114ºC for JSC-1A, 1242ºC respectively for NU-LHT-4M, and 1212ºC for CSM-LHT-1G (thermocouple accuracy in that range is ±0.75%). Strictly speaking, decrepitation is expected to occur at lower than melting temperatures due to crystal defects and weakening of the crystal structure failing under internal pressure from supercritical fluids in the vesicular inclusions. For the purpose of this investigation, however, the difference between the decrepitation and melting temperatures was not significant. Note that the value for JSC-1A (1114±8ºC) did not deviate significantly from the 1126ºC for JSC-2A, derived from calorimetric studies (Zocca et al., 2020). (JSC-2A was produced by Zybek Advanced Products, Inc., as a replica of JSC-1A from the same Merriam Crater basaltic source.)

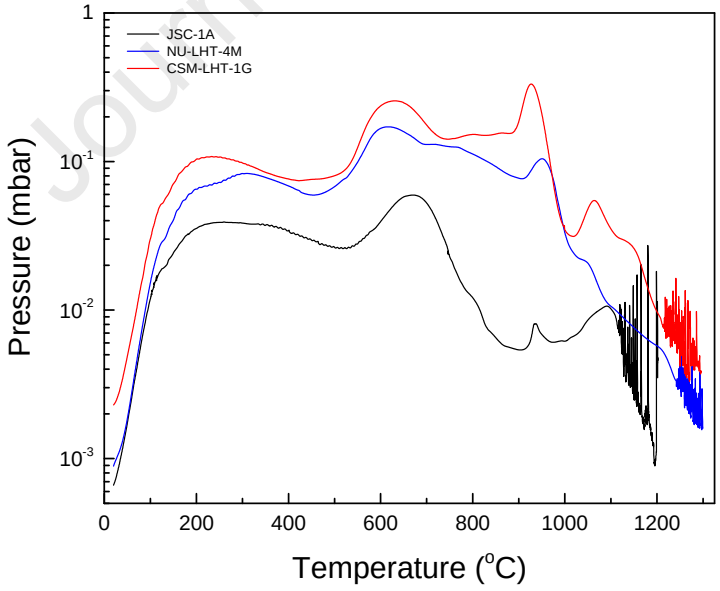

Figure 2. Pressure-temperature profiles for approximately equal amounts of JSC-1A (black), NU-LHT-4M (blue), and CSM-LHT-1G (red) lunar regolith simulants. The pressure spikes, attributed to decrepitation events, mark the respective melting temperatures.

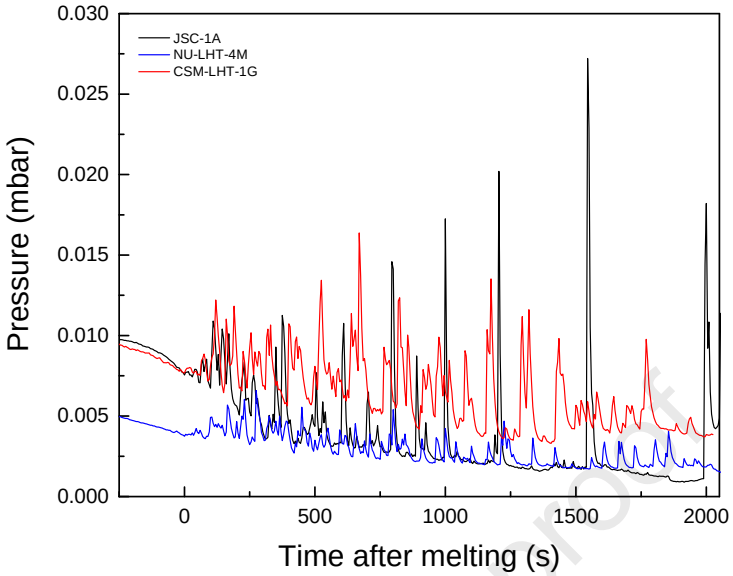

Figure 3. Decrepitation pressure spikes as a function of time, plotted for each sample from the onset of decrepitation. Line colors for JSC-1A (black), NU-LHT-4M (blue), and CSM-LHT-1G (red) correspond to these in **Figure 2**.

It must be noted that the pressure within the sample is not a property of the system, but rather an intrinsic characteristic of the man-made regolith simulant, governed by its own gas load it generates during heating. High-conductance systems can be constructed to allow fast evacuation of that gas load from small samples and maintain high vacuum continuously (e.g., Cardiff et al, 2007); however, the intrinsic sample pressure in bulk media would be determined by the percolation rate of the evolving gases through the powder, which occurs in laminar flow conditions. A rough estimate of the gas throughput resulting in 0.01 mbar pressure at the sample in our system yielded ~2 atm.-cm^3/s (Petkov & Voecks, 2023). For similar viscous flow conditions within bulk simulant powder, the highest pressure in **Figure 2** corresponds to a gas load of several atm.-cm^3/s per gram of regolith sample. This demands an adequate consideration for ISRU technologies whose validation requires 10s or 100s of kilograms of regolith.

Gas release from decrepitation events did not amount to a significant contribution to the total quantity of gas evolving from a regolith simulants sample during vacuum heat treatment. **Figure 3** shows a direct comparison of the respective pressure profiles from the onset of melting for each individual sample. To aid an approximate estimate, the integral area under the decrepitation peaks was estimated by subtracting the respective "floor" of the pressure trend. The results were ~0.5%, ~0.05% and 0.15% of the cumulative gas quantity evolved from JSC-1A, NU-LHT-4M and CSM-LHT-1G, respectively. It is acknowledged that the data acquisition was not optimized for monitoring the fast pressure spikes, which led to a moderate underestimate. The limited conductance at the sample caused prolonged pumping of the gas bursts, allowing to evaluate the upper bound for that ambiguity through peak shape analysis. The decrepitation gases in the case of JSC-1A exceeded the estimate from the integral by no more than 50%. Owed to the lower conductance setting for the other two samples (see Section

2), the more extended pumping of their volatiles resulted in a smaller overestimate. It can thus be deduced that decrepitation gases accounted for 0.1-1% of the total evolved gases form the studied lunar regolith simulants. Volatile decomposition byproducts of non-lunar components represent the largest gas threat to vacuum processing of man-made lunar regolith simulants.

3.4 Comparison of Volatiles Evolved During In-Vacuo Heating

Volatile gas signatures were monitored continuously by the RGA. The species were identified by their fragmentation patterns (NIST database). Cumulative thermal profiles, corresponding to H_2, H_2O, NO, H_2S, CO_2, SO_2, SO_3, HCl, and HF, were generated per the procedure described by Petkov & Voecks (2023). The constructed profiles assume equal gas detection efficiencies (N_2 equivalent, as commonly expressed in vacuum science). For the species above, the inaccuracy can exceed a factor of two, leading to underrepresentation (for H_2) or overrepresentation (for sulfur compounds) of their contribution to an RGA spectrum. This work rectifies that by scaling the individual thermal profiles with the respective sensitivities given in **Table 1**. Such correction factors (e.g., MKS Instruments) arise from differences in the molecular ionization cross-sections induced by the (75 eV) electrons of the RGA ion source. These values are similar to gas correction factors for ionization gauges (Bartmess and Georgiadis, 1983), utilizing the same phenomenon. (Note that the NO trace was scaled with the correction factor for NO_2 considered to be the parent molecule generated during nitrate decomposition. NO_2 was not conclusively identified due to high organic background at m/z=46 at low temperatures.) The resulting profiles for JSC-1A, NU-LHT-4M and CSM-LHT-1G are shown as a collage of plots with identical scales for direct comparison (**Figure 4**). The total pressure corresponds to N_2 equivalent and carries no gas correction at any stage; it does not represent the integral of all gas specific RGA traces.

Table 1. RGA sensitivity for different gases with respect to N_2, shown within two significant digits.

Species	H_2	H_2O	NO	H_2S	CO_2	SO_2	HF	HCl
Gas correction factor	0.44	1.0	1.5*	2.2	1.4	2.1	1.4	1.6

*The 1.5 correction factor for NO_2 parent was used instead of 1.2 for NO.

Water dominated the volatile constituents produced during the heating process of all regolith simulants to 900-1000ºC. Physisorbed water on particle surfaces (~1 m^2/g) accounted for only a small fraction of the total quantity at lower temperatures (≲300-350ºC). Most of the water was generated by dehydration of the regolith. Dehydration (Kim and Lee, 2013), regardless of the specific source (hydrates, hydrous oxides, clays, etc.), encompasses the removal of H_2O and OH^- species form materials. Water (steam) becomes highly reactive at elevated temperatures and can act as either reducing or oxidizing reagent. This promotes a diverse range

of secondary reactions, the byproducts of which create a complex gaseous environment within regolith simulants that is difficult to decode.

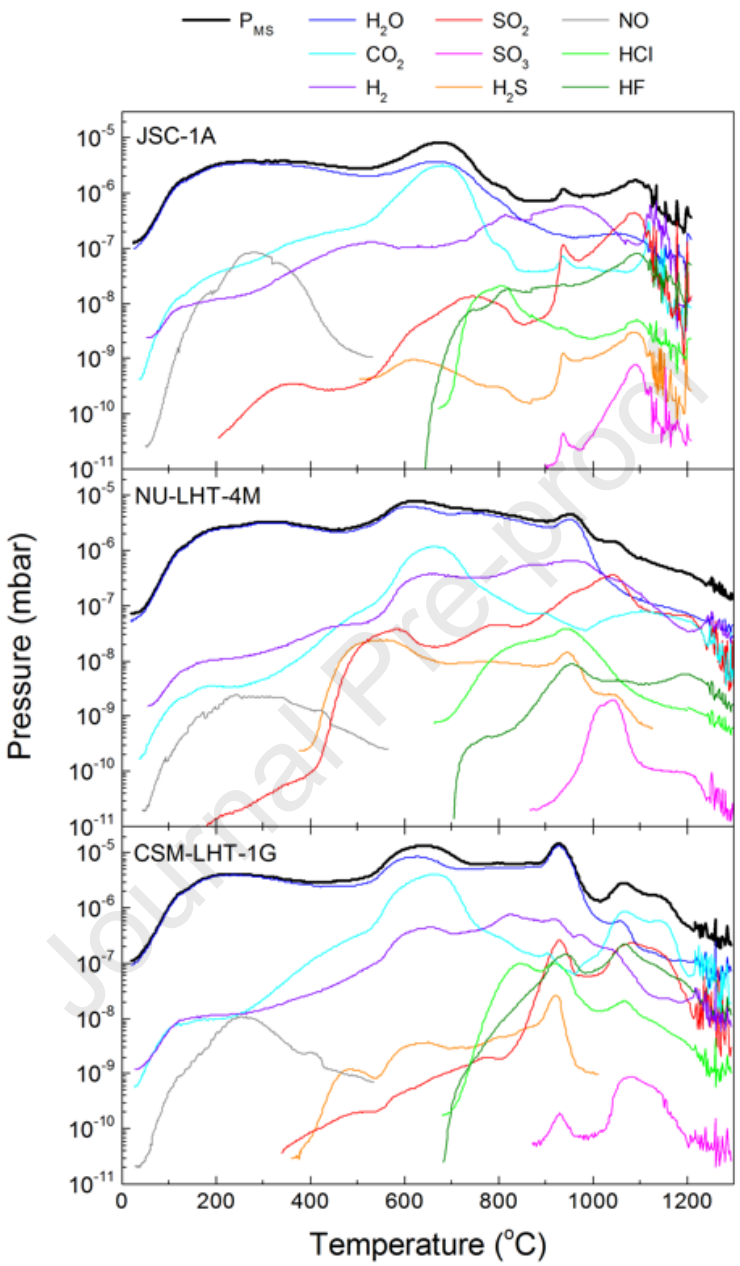

Figure 4. RGA traces of H_2O (blue), CO_2 (cyan), H_2 (purple), SO_2 (red), SO_3 (magenta), H_2S (orange), HCl (green), HF (olive), and NO (grey), given for JSC-1A (top), NU-LHT-4M (middle) and CSM-LHT-1G (bottom plot) on the same scale. The traces, scaled using the correction factors from **Table 1**, are shown only in the regions where the respective species were conclusively identified by MS. Note that the total RGA pressure (respective black lines), measured by an ionization gauge, is shown as N_2-equivalent, not the integral of all traces..

Strong CO_2 signatures in the RGA data were observed in all simulants. That was attributed to decomposition of carbonate minerals, such as calcite, dolomite, or siderite. Calcite has been the most commonly identified carbonate in simulants, and is probably the dominate carbonate in these simulants, although dolomite and siderite are also known in NU-LHT-4M. In its pure crystalline form, decomposition of calcite proceeds rapidly above 750ºC (Karunadasa et al., 2019). The strong CO_2 presence at lower temperatures could be attributed to constituents in the self-generated gaseous environment. High-temperature water vapor (steam) is known to promote catalytic decomposition of carbonates (Giammaria and Lefferts, 2019), whereas partial CO_2 pressure can also influence the $CaCO_3$ decomposition rate (Galan et al., 2013).

Carbonates are either totally absent or extremely rare on the Moon. Therefore, removal of carbonates that are present in lunar ens may be desirable to increase their fidelity for some applications. This is achievable via thermal decomposition, which is limited by the crystallization temperatures of relevant glasses, being ~750ºC. Such treatment is not conducive to removing other regolith constituents that give origin to CO_2 resulting from other reactions occurring at higher temperatures (>1000ºC). CO_2 of primary volcanic origin can also exist in glasses or can be trapped at high-pressures in vesicles. These forms of existence of CO_2 in the simulants are not undesirable, as they are expected to be present in lunar regolith.

Multiple RGA signatures (H_2S, SO_2, SO_3) indicate volatilization of sulfur via oxidation or reduction reactions. Sulfur in the simulants can exist in multiple forms. Various primary sulfides, which are known lunar minerals, are known to exist in JSC-1A, NU-LHT-4M, and CSM-LHT-1G. The most prevalent sulfide is pyrite, FeS_2, an analog for the troilite, FeS, in lunar samples. The simulant's self-generated environment produced small amounts of reduced sulfur (H_2S), which could be attributed generally to pyrite, and in the case of NU-LT-4M, also to pyrrhotite. H_2S can also be extracted directly from primary volcanic glass above its crystallization temperature (~750ºC).

Sulfur can also exist in the form of sulfates, SO_4^{2-}. JSC-1A and CSM-LHT-1G are almost certain to also have sulfates, especially gypsum, $CaSO_4 \cdot 2H_2O$, and possibly bassanite, $2CaSO_4 \cdot H_2O$. Decomposition of sulfates generates SO_2 and some SO_3 in proportions depending on the mineral types (Lau et al., 1977). Gypsum (or bassanite) produces mainly SO_2 and trace amounts of SO_3, that latter becoming detectable only at high temperatures. Reactions of sulfates with the self-generated environment may facilitate decomposition at lower temperatures than those for the pure crystalline materials, but the experimental evidence implies that sulfates are largely unaffected below the typical glass crystallization temperatures. This presents a challenge for devising a strategy to remove the non-lunar sulfur components from simulants in order to improve the simulant fidelity. Bakeout in reducing environment (Wilkerson et al., 2023) may promote sufficient removal of sulfates.

Elemental hydrogen is not found in mineral lattice except as hydroxyl or ammonia radicals, or as H_2O such as waters of hydration. H_2O can also exist as molecular water trapped on or within large defects in the crystal lattice called fluid inclusions. Hydrogen exhibited a strong presence in the RGA spectra of the investigated simulants, especially at higher temperatures. H_2, occurring at different temperature ranges, can be produced by a range of primary and secondary reactions, especially from secondary phases, such as clay minerals and gypsum. Trends of the H_2 signatures can be correlated to other volatiles, but mass spectrometry alone does not provide conclusive evidence of chemical reactions in the simulant materials.

Minor but noticeable volatile constituents included NO_2 (by virtue of NO detection below 550-600ºC), HCl and HF. Chlorine and fluorine bearing compounds give rise to the HCl and HF signatures detected in all simulant materials at temperatures above ~700ºC. Reduced Cl (HCl) and F (HF) in our data are probably derived from any number of primary chlorine- and fluorine-bearing minerals, such as apatite, muscovite, or augite. The mixture of minerals, the diversity of their form, and the complex self-generated gas environment can promote a multitude of thermal reactions generating HF and HCl.

Nitrogen compounds in the simulants are almost certainly from contaminants in the simulants. Such contaminants can come from either biological processes in the natural environment mined as source for the simulant, or various contaminants derived from the mining or milling processes, such as spilled engine oils, residue of blasting, or plastic insulation on blasting cord. A range of other notable, albeit minor contributors to the RGA spectra, include O_2, byproducts of nitrates decomposition.

The detection of NO above 900ºC was intriguing. The organic background, which prevented the detection of NO_2 at lower temperatures, was greatly reduced; however, no NO_2 correlated with the NO signature was registered. This alludes to NO being a byproduct of nitrides reacting with oxidizing agent from the self-generated environment (e.g., steam). The reaction is likely reversible. After cooling the thermally processed regolith to room temperature, exothermic reaction occurred upon exposure to pure N_2 gas. The generated heat was most pronounced in the JSC-1A simulant (samples exceeded 100ºC). Further investigation is warranted.

476 ### 3.5 Mass loss quantification

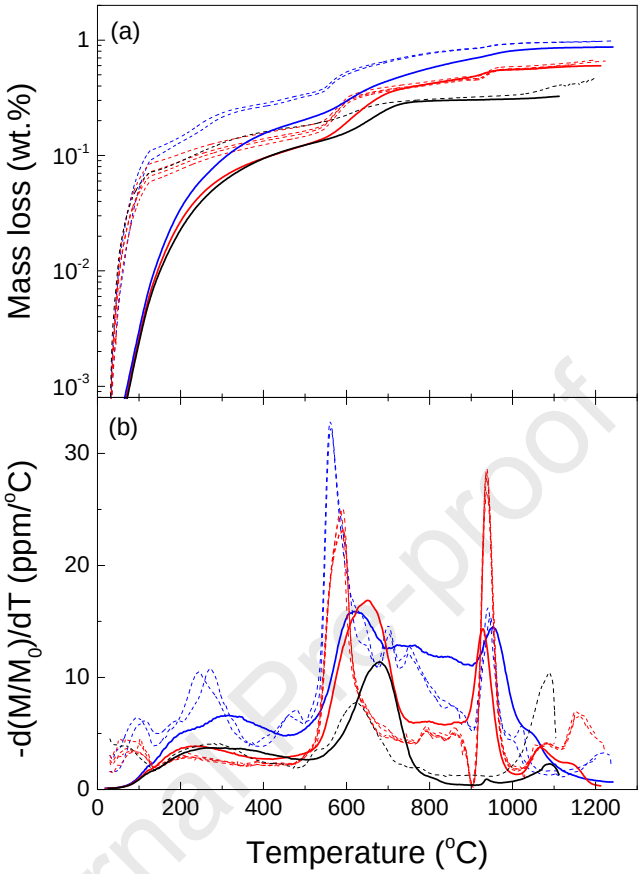

477 **Figure 5**. Total (a) and differential mass loss (b) calculated from TGA (dotted lines) and MS
478 (solid lines) for JSC-1A (black), NU-LHT-4M (blue) and CSM-LHT-1G (red). Multiple TGA
479 data sets shown for NU-LHT-4M and CSM-LHT-1G attest to a very good reproducibility. The
480 integral MS mass loss between 150ºC and the respective melting temperatures were normalized
481 to the respective TGA values.

482 Mass loss quantification of the investigated lunar regolith simulants was based on TGA,
483 complemented by MS, providing information on individual regolith components. **Figure 5**
484 compares the total (a) and differential mass loss (b), calculated from TGA (dotted lines) and MS
485 (solid lines) for JSC-1A (black) NU-LHT-4M (blue) and CSM-LHT-1G (red). To minimize
486 initial moisture outgassing effects in vacuum at room temperature prior to the start of the
487 experiments, the TGA results were zeroed at 30ºC. Multiple spectra shown for the latter two
488 simulants (dotted lines, not intended to be resolved individually in this plot) exemplify the high
489 sample-to-sample reproducibility owed to the large sample size under test. The TGA data show
490 higher mass loss from NU-LHT-4M compared to CSM-LHT-1G, which has not been reconciled
491 with their outgassing profiles obtained at identical conditions with the present system (**Figure 2**).
492 Due to recognized uncertainties of the latter technique, causing ambiguities in direct mass
493 quantification, MS is used here as complementary to TGA. To this end, total mass loss profiles
494 were calculated as the sum of the individual volatile species shown in **Figure 4** weighted with
495 the corresponding mass, and the results were normalized to the respective TGA integral values
496 from 150ºC to the respective regolith melting temperatures. The choice of 150ºC (above the end

of the 1ºC/min heating rate) was rooted in typical vacuum bakeout temperatures intended to minimize variability due to physisorbed moisture. It must be noted that the mass losses were dominated by moisture removal, and degradation of carbonates and sulfur compounds. The cumulative mass loss of all minor components from **Figure 4** (H_2, H_2S, NO_2, HCl and HF) did not exceed 0.01 wt.% for any of the tested samples. The unaccounted in Fig. 3 balance in the RGA spectra (mostly from organic volatiles) contributed significantly less than 0.01 wt.% to the total mass loss.

Figure 5(b) compares the differential mass loss from TGA and MS. The MS data exhibit broader, less defined peaks with similar onsets. This attests to inertial effects due to gas transport through the sample bulk, and subsequently from the furnace to the spectrometer through a path with limited conductance. Consideration must be given to the species dependence of such gas transport through the different sticking coefficients and resident times for molecules interacting with surfaces of particles and system walls (e.g., H_2O, SO_2/SO_3), whose transport would exhibit greater delay than that of non-interacting gases (e.g., H_2, CO_2).

The normalization factors for JSC-1A, NU-LHT-4M, and CSM-LHT-1G obtained from the scaling of the cumulative MS and TGA mass loss values adopted for **Figure 5** were used to scale the contribution of the individual species evolving from each regolith simulant. The high MS dynamic range allowed for investigation of volatiles evolving from trace elements. The integral mass loss profiles for H_2O (blue), CO_2 (cyan), SO_3 (red), HCl (green), HF (olive), and NO_2 (grey) are shown as a function of temperature in **Figure 6**. The data for JSC-1A (solid line), NU-LHT-4M (dashed line), and CSM-LHT-1G (dash-dotted line) extend to the respective melting temperatures. Dehydration, in its prevalent general definition of H_2O and OH^- removal, dominated the mass loss for all tested regolith simulants. The reader is reminded that the data presented here have minimum contribution from physisorbed moisture, the majority of which was removed through extended pumping prior to the start of the experiments. Due to the mineralogical complexity and the myriad of H_2O and OH^- sources in the regolith composition, the discussion of specific processes (e.g., dehydration of hydrates, dihydroxylation, etc.) falls outside the scope of this work. Decomposition products of carbonates, sulfates and sulfur compounds, represented at different proportions in the studied regolith simulants, constitute the other major contributors to the mass loss.

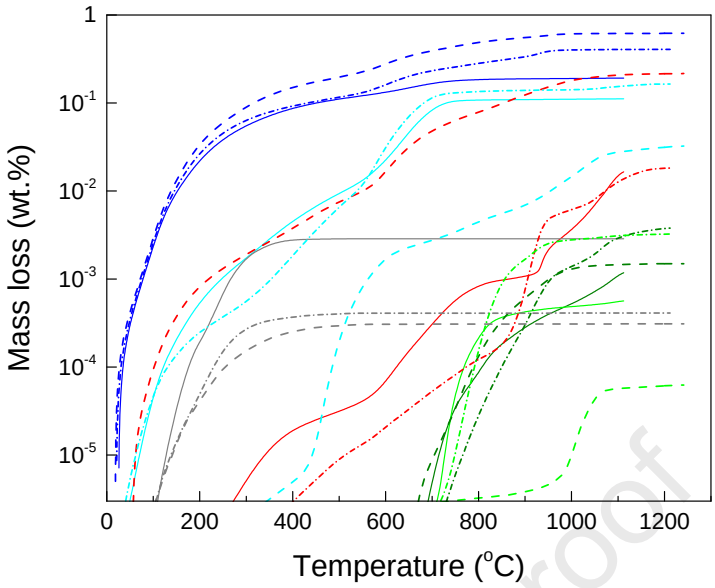

527

528 **Figure 6**. Mass loss of individual regolith components as a function of temperature: H_2O (blue),
529 CO_2 (cyan), SO_3 (red), HCl (green), HF (olive), and NO_2 (grey). The regolith simulants are
530 represented as follows: JSC-1A (solid lines), NU-LHT-4M (dashed lines) and CSM-LHT-1G
531 (dash-dotted lines).

532

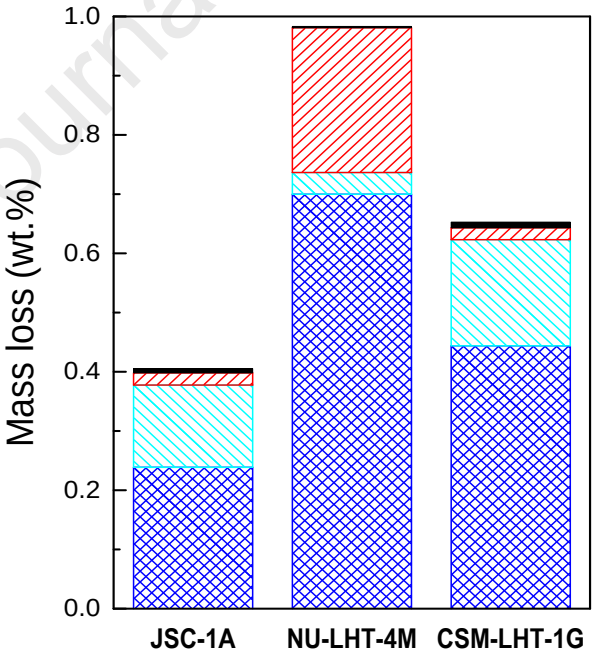

533

534 **Figure 7**. Cumulative mass loss attributable to dehydration (blue, cross-hatch), decomposition
535 of carbonates (cyan, left-hatch) and sulfates (red, right-hatch) and other minor contributors
536 (nitrates, fluorine and chlorine bearing compounds, etc.; solid black).

It is worth considering vacuum heat treatment with respect to the typical crystallization temperatures of volcanic glasses (~750ºC), which limits the heat exposure of the simulant in order to avoid considerable adverse morphological changes. At such temperatures, nitrates and other N-contaminants are fully degraded by 400ºC, and volatile organic compounds (not presented here) are decomposed or combusted at temperatures <600ºC. Carbonates decomposition can be complete given sufficient time, whereas sulfates remain largely unaffected. F- and Cl-bearing minerals that give rise to HCl and HF at >700ºC are also difficult to remove by that stage. Vacuum thermal processing of simulant materials at ~750ºC is a viable approach for removing a large fraction of the non-lunar phases, but some of them would require different approaches.

Figure 7 illustrates the comparison among the three regolith types in the form of a stacked bar chart of the integral mass loss contributions from dehydration (blue, cross-hatched area), decomposition of carbonates (cyan, left-hatched) and sulfur compounds (red, right-hatched), and aggregate contribution from degradation of all other trace components (black, solid). The cumulative mass loss values prior to melting of the respective simulant were 0.41 wt.% for JSC-1A, 0.98 wt.% for NU-LHT-4M, and 0.65 wt.% for CSM-LHT-1G. The reader is reminded that these values do not account for the surface moisture accumulated during simulants storage at ambient conditions; most of that has been removed during the vacuum conditioning of the sample prior to conducting these experiments (Petkov &Voecks, 2023). Accounting for the differences in experimental conditions, the above values are in good concurence with reported by Isachenkov et al. (2022) TGA-derived mass loss of LHS-1 (1.1 wt.%) and LMS-1 (1.38 wt.%) lunar regolith simulants made by Exolith Labs.

4 Results and Discussion – Part B: Analysis of CSM-LHT-1G in the Context of its Individual Components

4.1 Individual CSM-LHT-1G Constituents

CSM-LHT-1G is comprised of four components – GreenSpar anorthosite (GSA), Merriam Crater basalt (MCB), VWR augite (Aug), and Washington Mills glass (WMG) with proportions given in Section 2.1. Samples weighing 10.00±0.02 g of each of the above were subjected to identical vacuum heat treatment to that of CSM-LHT-1G. The gas flow fraction to the MS was kept identical (29%) to aid the direct comparison at the expense of suppressed sensitivity to trace components evolving from the MCB and WMG samples. The MS data were analyzed according to the procedure in Section 3.2. Owing to the identical measurement conditions, no normalization was necessary. The results are presented as a collage in **Figure 8**, with each individual plot having the same temperature and pressure scale for a direct comparison.

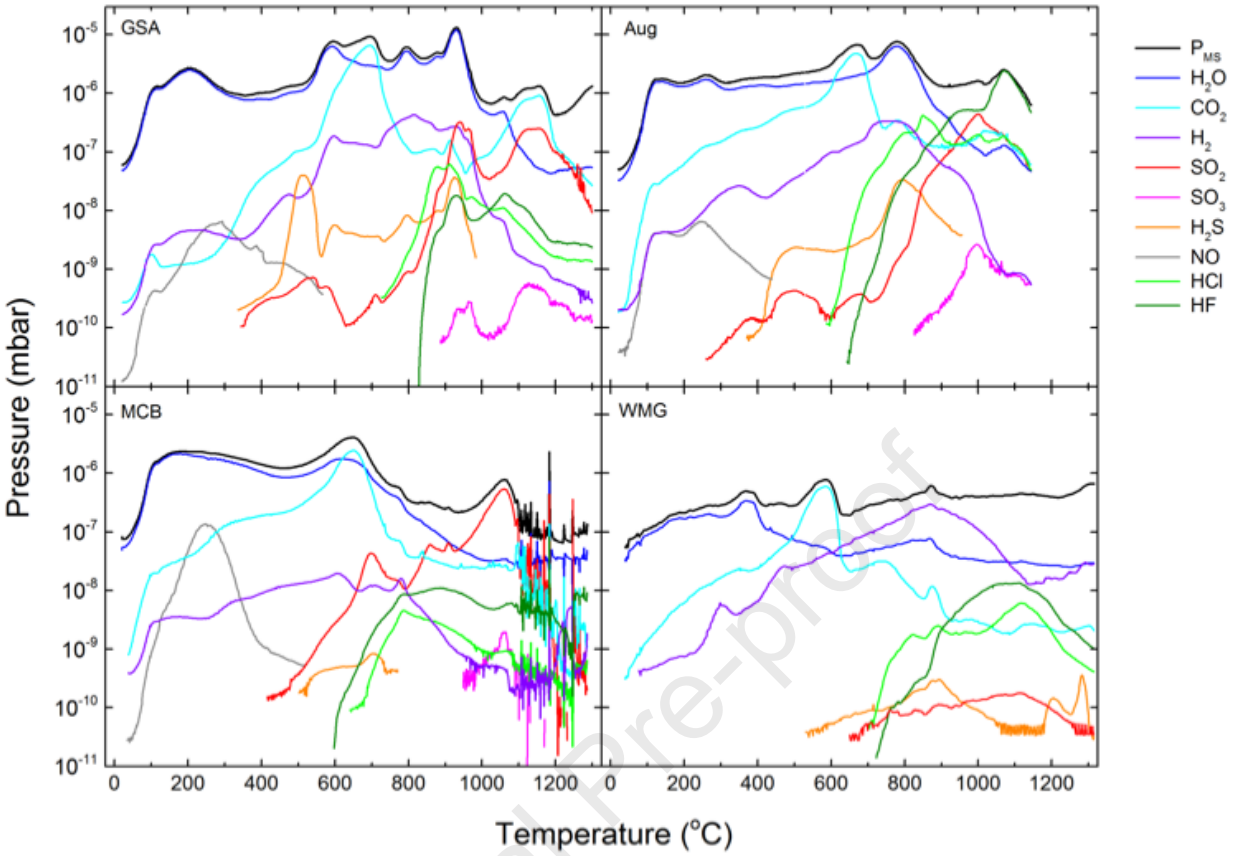

Figure 8. RGA traces as a function of temperature for the four CSM-LHT-1G components – GSA, MCB, Aug and WMG. The color scheme is identical throughout this paper: H_2O (blue), CO_2 (cyan), H_2 (purple), SO_2 (red), SO_3 (magenta), H_2S (orange), HCl (green), HF (olive), and NO (grey).

A notable deviation from the previous analysis (Section 3.2) was necessitated by the observed strong SiF_4 presence produced by the augite sample at temperatures above 1000ºC. The origin of SiF_4 was traced to a secondary reaction of HF, generated by impurities in the augite, with the quartz vessel. The reaction was substantiated by the subsequent observation of large etch pits in the quartz reactor walls. At the maximum SiF_4 signature at 1070ºC, the HF-related RGA contribution (SiF_4 and HF) amounted to >70% of the entire RGA spectrum. To properly account for all HF generated by the augite, the main peak (m/z=85) was scaled to the total SiF_4 amount according to its fragmentation pattern (NIST database), the SiF_4 signal was then adjusted with its ionization coefficient (0.35 per Bartmess & Georgiadis, 1983), and the cumulative HF contribution was obtained as the sum of the HF and $4\times SiF_4$ traces (according to the reaction $SiO_2 + 4HF \rightarrow SiF_4 + 2H_2O$). The resulting profile (**Figure 8, Aug**) accounts for the majority of the total pressure at 1070ºC. Although faint m/z=85 peaks were detected in some other spectra, no SiF_4 correction was necessary for any other simulant material or simulant constituent.

The augite experiment was terminated at a lower temperature due to a failure of the furnace control thermocouple. A repeat of the experiment was undesirable due to the strong HF generation and was deemed unnecessary for the purpose of this work.

Pertinent to oxygen extraction experiments from anorthosite-rich lunar regolith, it is worth mentioning that the increase in the total pressure in the GSA sample at >1200ºC was caused solely by O_2 (not detailed in this work). Oxygen was the only significant RGA constituent that had an increasing trend at such temperatures.

4.2 Comparison of CSM-LHT-1G with a Weighted Superposition Spectrum of its Components

The CSM-LHT-1G component with the highest outgassing rate per unit mass was the anorthosite, followed by the augite, basalt, and glass. The outgassing from the glass is at least an order of magnitude lower than that of the other components and is therefore not a major contributor to the volatiles evolving from the composite. This assessment of the RGA profiles of the individual constituents allow for identification of the source of some decomposition products in the composite regolith. To this end, a composite spectrum was produced by calculating the weighted average for each of the traces shown in **Figure 8** with the weight fraction of the respective component in the CSM-LHT-1G composite (Section 2.1). The resulting composite spectrum was compared to that of CSM-LHT-1G in **Figure 9**. No adjustment for the different weights of the 23.4 g CSM-LHT-1G sample and the 10 g "composite sample" was deemed necessary for the intended qualitative comparison. Larger samples under test generally exhibit broader peaks due to the slower gas percolation through the powder bulk. This is corroborated by the comparison of the JSC-1A spectra in **Figure 4** (23.1 g) and that in **Figure 8** (10 g).

The volatile signatures in the actual and reconstructed spectra exhibit strong similarities. The dehydration, particularly the initial range (<400ºC) and around the ~930ºC peak, are adequately recreated. The 550-850ºC range is also replicated reasonably well, apart from the more detailed H_2O peak structure with individual peaks attributable predominantly to the anorthosite and basalt. Such details might be unresolvable in the larger CSM-LHT-1G sample. Alternatively, the local mineralogical environment in individual components might influence the temperatures at which some reactions occur. An excellent correspondence was also observed in the comparison of the CO_2 signatures. The qualitative comparison of the remaining volatile trends also shows reasonably good correlations. The overall quantitative comparison was also well replicated. This can be seen in the intensities of the NO (<400ºC), the SO_2 and H_2S production at high temperatures, and the HCl and HF generation at >700ºC. Despite its small (6 wt.%) fraction in the composite, augite appears to be a dominant source of HF in the CSM-LHT-1G simulant. The fluorine-bearing compounds can be attributed to fluorite impurities in the augite. Impurities in the minerals can play a significant role in mass spectrometry when the dominant species are stable in the given temperature range. The glass powder, which has been prepared from high purity glass, also exhibited uncharacteristically strong outgassing above its vitrification temperature likely due to impurities introduced during milling.

632

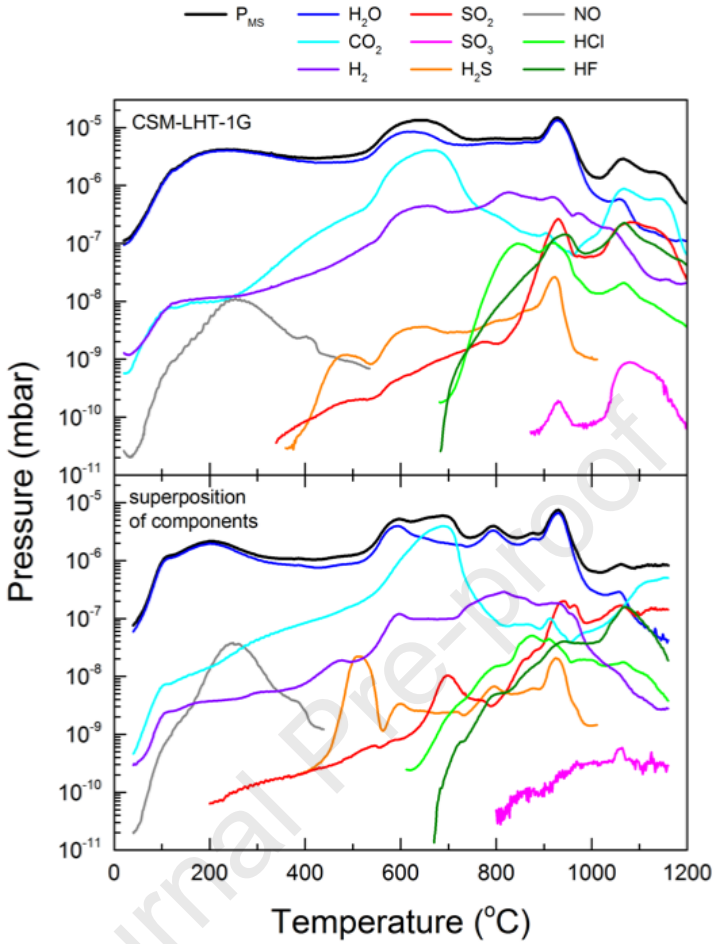

633 **Figure 9**. Comparison of RGA traces as a function of temperature of CSM-LHT-1G and a
634 synthetic spectrum of its components, weighted with their respective fraction. Identical color:
635 H_2O (blue), CO_2 (cyan), H_2 (purple), SO_2 (red), SO_3 (magenta), H_2S (orange), HCl (green), HF
636 (olive), and NO (grey).

637

638 The limitation of the superposition approach was illustrated by the weak SO_3 signal,
639 which failed to reproduce relevant details. The decomposition of gypsum produces SO_3 from the
640 surface and SO_2 from the bulk of the mineral particles (Lau et al., 1977) with proportions
641 expectedly corresponding to the mean surface to volume ratio of the gypsum particles in the
642 simulant. That proportionality is evident in the CSM-LHT-1G spectrum (**Figure 9**), as well as in
643 those of the anorthosite, augite and basalt components (**Figure 8**). The reconstruction of the
644 ~1000 times fainter signal, however, was hindered by the more restricted flow rate to the MS for
645 the lower outgassing components (MCB and WMG), adopted for the direct comparison.
646 Nonetheless, component analysis proved useful for identifying sources of specific volatiles
647 evolving from the CSM-LHT-1G.

5 Conclusions

This work compares volatiles evolving from lunar regolith simulants to inform *in vacuo* thermal processing activities. The investigated materials were high-fidelity mare (JSC-1A) and highland (NU-LHT-4M) lunar regolith simulants, as well as a CSM-LHT-1G – a recently developed highland simulant, available in sufficient quantities for large-scale technology development in support of NASA's Artemis program. In addition to known mineralogical differences, the behavior of man-made simulants heated under vacuum can deviate significantly from that of lunar regolith even when lunar conditions are replicated. All simulants generated large gas loads [~1 atm.-cm^3/(s·g)], significantly more pronounced in the highland simulants. This self-generated environment comprises the decomposition products of simulant components, most of which have non-lunar origin, and a complex combination of primary and secondary reactions of the products.

The self-generated environment generated during *in vacuo* heating was dominated by water in the form of H_2O and OH^-, released by minerals and clays. The other major contributors to the evolving gases were CO/CO_2, primarily from the decomposition of carbonates, and SO_2/SO_3 mainly from decomposition of sulfates and sulfides. Sulfates/sulfides and carbonates were represented in various quantities in the different simulants. Reduced sulfur in the form of H_2S, likely originating from pyrite and pyrrhotite, was also observed albeit in smaller quantities. Minor but noticeable constituents of the self-generated environment were attributed to impurities in the main minerals, or other contamination. These include HF and HCl, generated by decomposition of trace-level fluorine- and chlorine-bearing minerals, and nitrogen, likely from biological or other process contamination. The achieved high dynamic range in the MS data presents an alternative to presently used complex trace element analysis techniques.

It must be noted that the correlation between the volume fraction of a given thermally degradable compound in the simulant, and the amount of volatile it generates during thermo-vacuum processing, are not necessarily directly correlated. The specifics are governed by its exposure to the environment, decomposition rates and temperature, and influences of other present volatiles and competing reactions. *In vacuo* thermal decomposition, however, offers an opportunity to remove or reduce the quantity of non-lunar phases from the man-made simulants at below glass crystallization temperatures. This can enhance the material fidelity.

Simulant material engineering can be aided by analysis of its individual constituents, as demonstrated here with the CSM-LHT-1G. Large quantities of undesirable HF were generated by the decomposition of fluorine-bearing compounds, likely fluorite impurities in the commercial augite, which was added to the simulant to better approximate the main lunar mineralogy. A different source of augite or a purification step prior to mixing may be advantageous.

The investigation approach presented in this work represents a valuable method for assessing the performance of man-made lunar regolith simulants at high temperatures in vacuum in preparation for a direct comparison to actual lunar regolith. It also reveals potential hazards (high gas loads, HF, HCl, etc.) that must be addressed during the development of large-scale testbeds for validation of lunar technologies.

Application of this method to authentic lunar regolith is of genuine interest. In the absence of secondary minerals found in Earth-sourced material, the enhancement of the MS dynamic range can feasibly advance the state-of-the-art in the investigation of trace elements in

lunar soil samples. Such research would benefit relevant ISRU technologies, which are being developed on Earth using man-made simulants, by deducing their expected performance characteristics in lunar environment.

Acknowledgements

This work, carried out in support of NASA's Moon-to-Mars Planetary Autonomous Construction Technology (MMPACT) project, was performed by the Jet Propulsion Laboratory, California Institute of Technology, under contract with the National Aeronautics and Space Administration (80NM0018D0004). Thermogravimetric analysis was performed at NASA Marshall Space Flight Center. Manuscript preparation and publication was supported by SuprAEther LLC.

Declaration of Competing Interest

The authors declare that they have no known competing financial interests or personal relationships that could have appeared to influence the work reported in this paper.

Data availability

Data is available on request from the corresponding author.

References

Aird H.M., and Boudreau, A.E. (2013). High-temperature carbonate minerals in the Stillwater Complex, Montana, USA. Contrib. Mineral Petrol (2013) **166**:1143–1160. https://doi.org/10.1007/s00410-013-0913-2.

Aird, H.M., Ferguson, K.M., Lehrer, M.L., and Boudreau, A.E. (2017). A study of the trace sulfide mineral assemblages in the Stillwater Complex, Montana, USA. Miner. Deposita **52**:361–382. https://doi.org/10.1007/s00126-016-0664-x.

Allen, C.C., Morris, R.V., and McKay, D.S. (1996). Oxygen extraction from lunar soils and pyroclastic glass. J. Geophys. Res. E Planets, **101**(E11) 26085–26095; https://doi.org/10.1029/96JE02726.

723 Altun, A., Ertl, F., Marechal, M., Makaya, A., Sgambati A., and Schwentenwein, M. (2021). Additive
724 manufacturing of lunar regolith structures. Open Ceramics, **5** 100058.
725 https://doi.org/10.1016/j.oceram.2021.100058.
726 Anderson, R.C., Beegle, L.W., Peters, G.H., Fleming II, G.M., Jandura, L., Kriechbaum, K., Manatt, K., Okon, A.,
727 Pounders, E., Sollitt, L., and Sunshine, D. (2009). Particle transport and distribution on the Mars Science
728 Laboratory mission: Effects of triboelectric charging. Icarus **204**(2) 545–557.
729 https://doi.org/10.1016/j.icarus.2009.07.006.
730 Bartmess, J.E., and Georgiadis, R.M., (1983). Empirical methods for determination of ionization gauge relative
731 sensitivities for different gases. Vacuum **33**(3), 149-153. https://doi.org/10.1016/0042-207X(83)90004-0
732 Boudreau, A.E. (2016). The Stillwater Complex, Montana – Overview and the significance of volatiles. Miner.
733 Magazine, **80**(4) 585–637; https://doi.org/10.1180/minmag.2016.080.063.
734 Cardiff E.H., Pomeroy, B.R., Banks, I.S., and A. Benz (2007). Vacuum Pyrolysis and Related ISRU Techniques.
735 AIP Conf. Proc.; **880** 846–848; https://doi.org/10.1063/1.2437525.
736 Cesaretti, G., Dini, E., DeKestelier, X., Colla, V., and Pambaguian, L. (2014). Building components for an outpost
737 on the Lunar soil by means of a novel 3D printing technology. Acta Astronaut., **93** 430–450;
738 https://doi.org/10.1016/j.actaastro.2013.07.034.
739 Farries, K.W., Visintin, P., Smith, S.T., and Eyk, P.v. (2021). Sintered or melted regolith for lunar construction:
740 state-of-the-art review and future research directions. Constr. Build. Mater., **296** 123627.
741 https://doi.org/10.1016/j.conbuildmat.2021.123627.
742 Galan, I., Glasser, F.P., and Andrade, C. (2013). Calcium carbonate decomposition. J. Therm. Anal. Calorim. **111**:
743 1197–1202. https://doi.org/10.1007/s10973-012-2290-x.
744 Giammaria, G., and Lefferts, L. (2019). Catalytic effect of water on calcium carbonate decomposition. J. CO2 Util.
745 **33**: 341-356. https://doi.org/10.1016/j.jcou.2019.06.017.
746 Goulas, A., and Friel, R.J. (2016). 3D printing with moondust. Rapid Prototyp. J. **22**(6), 864–870.
747 https://doi.org/10.1108/RPJ-02-2015-0022.
748 Guerrero-Gonzalez, F.J., and Zabel, P. (2023). System Analysis of an ISRU Production Plant: Extraction of Metals
749 and Oxygen from Lunar Regolith. Acta Astronaut., **203**, 187–201.
750 https://doi.org/10.1016/j.actaastro.2022.11.050.

Gustafson, R.J., White, B.C., Gustafson, M., and Carter, J.L. (2006). Development of Improved Lunar Regolith Simulants. In Planetary and Terrestrial Mining Sciences Symposium (3rd), June 4-6, Sudbury, Ontario: NORCAT, 2006.

Heiken, G.H., Vaniman, D.T., and French, B.M. (1991). Lunar Sourcebook: a user's guide to the moon. Cambridge University Press.

Howe, A.S., Wilcox, B., McQuin, C., Mittman, D., Townsend, J., Polit-Casillas, R., and Litwin, T. (2014). Modular Additive Construction Using Native Materials. Earth Sp. 2014 Eng. Extrem. Environ. - Proc. 14th Bienn. Int. Conf. Eng. Sci. Constr. Oper. Challenging Environ. 301–312 https://doi.org/10.1061/9780784479179.034.

Isachenkov, M., Chugunov, S., Akhatov, I., and Shishkovsky, I. (2021). Regolith-based additive manufacturing for sustainable development of lunar infrastructure – An overview. Acta Astronaut. **180** 650-678. https://doi.org/10.1016/j.actaastro.2021.01.005.

Isachenkov, M., Chugunov, S., Landsman, Z., Akhatov, I., Metke, A., Tikhonov, A., and Shishkovsky, I. (2022). Characterization of novel lunar highland and mare simulants for ISRU research applications. Icarus **376** 114873; https://doi.org/10.1016/j.icarus.2021.114873.

Karunadasa, K.S.P., Manoratne, C.H., Pitawala, H., Rajapakse, R.M.G. (2019). Thermal decomposition of calcium carbonate (calcite polymorph) as examined by in-situ high-temperature X-ray powder diffraction. J. Phys. and Chem. of Solids **134**: 21–28; https://doi.org/10.1016/j.jpcs.2019.05.023.

Kim, H.N., and Lee, S.K. (2013). Atomic structure and dehydration mechanism of amorphous silica: Insights from ^{29}Si and ^{1}H solid-state MAS NMR study of SiO_2 nanoparticles. Geochim. et Cosmochim. Acta **120**(1) 39–64; https://doi.org/10.1016/j.gca.2013.05.047.

Krishna Balla, V., Roberson, L.B., O'Connor, G.W., Trigwell, S., Bose, S., and Bandyopadhyay, A. (2012). First demonstration on direct laser fabrication of lunar regolith parts, Rapid Protot. J., **18**(6) 451-457; https://doi.org/10.1108/13552541211271992.

Krūmiņš, J., Kļaviņš, M., Ozola-Davidāne, R., and Ansone-Bērtiņa, L. (2022). The Prospects of Clay Minerals from the Baltic States for Industrial-Scale Carbon Capture: A Review. Minerals **12**(3): 349; https://doi.org/10.3390/min12030349.

Lau, K.H., Cubicciotti, D., and Hildenbrand, D.L. (1977). Effusion studies of the thermal decomposition of magnesium and calcium sulfates. J. Chem. Phys. **66**: 4532. https://doi.org/10.1063/1.433707.

779 Lemelin, M., Lucey, P.G., Song, E., and Taylor, G.J. (2015). Lunar central peak mineralogy and iron content using
780 the Kaguya Multiband Imager: Reassessment of the compositional structure of the lunar crust. J. Geophys. Res.
781 Planets, **120**: 869–887; https://doi.org/10.1002/2014JE004778.
782 MKS Instruments: "Spectra RGA Application Bulletin #208", p.2 "Ionization probability".
783 https://www.mks.com/mam/celum/celum_assets/resources/SpectraBulletin208.pdf (accessed: 1/20/2024).
784 NASA (2020). "Artemis Plan: NASA's Lunar Exploration Program Overview". https://www.nasa.gov/wp-
785 content/uploads/2020/12/artemis_plan-20200921.pdf?emrc=f43185.
786 NASA (2024) Astromaterials Research & Exploration Science https://ares.jsc.nasa.gov/projects/simulants/, and
787 https://ares.jsc.nasa.gov/projects/simulants/development-lab.html (last accessed August 2024.)
788 NIST Standard Reference Database 69: NIST Chemistry WebBook. https://doi.org/10.18434/T4D303.
789 Petkov, M.P., and Voecks, G.E. (2023). Characterization of volatiles evolved during vacuum sintering of lunar
790 regolith simulants. Ceram. Int. **49**(21) 33459-33468; https://doi.org/10.1016/j.ceramint.2023.06.178
791 Rasera, J., Cilliers, J., Lamamy, J., and Hadler, K. (2020). The beneficiation of lunar regolith for space resource
792 utilisation: A review. Planet. Space Sci., **186**, 104879; https://doi.org/10.1016/j.pss.2020.104879
793 Schlüter, L., and Cowley, A. (2020). Review of techniques for In-Situ oxygen extraction on the moon. Planet. Space
794 Sci., **181** 104753; https://doi.org/10.1016/j.pss.2019.104753.
795 Stoeser, D.B., Rickman, D.L., and Wilson, S.A. (2010). Design and Specifications for the Highland Regolith
796 Prototype Simulants NU-LHT-1M and -2M. NASA Technical Memorandum, NASA/TM—2010–216438: 24p.
797 https://ntrs.nasa.gov/api/citations/20110008071/downloads/20110008071.pdf.
798 Street, K.W., Ray, C., Rickman, D., and Scheiman, D.A. (2010). Thermal Properties of Lunar Regolith Simulants.
799 NASA Technical Memorandum, NASA/TM—2010-216348, May 1, 2010.
800 https://ntrs.nasa.gov/api/citations/20100024178/downloads/20100024178.pdf.
801 Suhaizan, M.S., Tran, P., Exner, A., and Falzon, B.G. (2023). Regolith sintering and 3D printing for lunar
802 construction: An extensive review on recent progress. Prog. Addit. Manuf., Article 537, 1-22;
803 https://doi.org/10.1007/s40964-023-00537-1.
804 Taylor, L.A., and Carrier, W.D. (1993). Oxygen Production on the Moon: An Overview and Evaluation. Resources
805 of near-earth space, Eds. J.S. Lewis, M.S. Matthews, and M.L. Guerrieri, Space Science Series. Tucson,
806 Arizona: The Univ. of Arizona Press, 1993, p.69

807 Taylor, L.A., and Meek, T.T. (2005). Microwave Sintering of Lunar Soil: Properties, Theory, and Practice. J.
808 Aerosp. Eng. **18**(3), 188–196 (2005). https://doi.org/10.1061/(ASCE)0893-1321(2005)18:3(188).
809 Toklu, Y.C., and Akpinar, P. (2022). Lunar soils, simulants and lunar construction materials: An overview. Adv.
810 Space Res, **70**(3) 762-779. https://doi.org/10.1016/j.asr.2022.05.017.
811 Washburn H.W., Wiley H.F., and Rock S.M. The mass spectrometer as an analytical tool. *Ind. Eng. Chem. Anal. Ed.*
812 **15** (1943) 541–547. https://doi.org/10.1021/i560121a001.
813 Whittington, A., and Parsapoor, A. (2022). Lower Cost Lunar Bricks: Energetics of Melting and Sintering Lunar
814 Regolith Simulants. New Space, **10**(2) 1–12. https://doi.org/10.1089/space.2021.0055.
815 Wilkerson, R.P., Petkov, M.P., Voecks, G.E., Lynch, C.S., Shulman, H.S., Sundaramoorthy, S., Choudhury, A.,
816 Rickman, D.L., and Effinger, M.R. (2023). Outgassing Behavior and Heat Treatment Optimization of JSC-1A
817 Lunar Regolith Simulant. Icarus **400** 115577. https://doi.org/10.1016/j.icarus.2023.115577.
818 Zhang, T.W., Ellis, G.S., Wang, K.S., Walters, C.C., Kelemen, S.R., Gillaizeau, B., and Tang, Y.C. (2007). Effect of
819 hydrocarbon type on thermochemical sulfate reduction. Org. Geochem. **38**(6) 897–910.
820 https://doi.org/10.1016/j.orggeochem.2007.02.004
821 Zocca, A., Fateri, M., Al-Sabbagh, D., and Günster, J. (2020). Investigation of the sintering and melting of JSC-2A
822 lunar regolith simulant. Ceram. Int., **46**(9) 14097-14104. https://doi.org/10.1016/j.ceramint.2020.02.212.

Declaration of Competing Interest

Comparison of Volatiles Evolving from Selected Highland and Mare Lunar Regolith Simulants During Vacuum Sintering

Mihail P. Petkov[1*], Ryan P. Wilkerson[2], Gerald E. Voecks[1], Douglas L. Rickman[3], Jennifer E. Edmunson[4], and Michael R. Effinger[4]

[1]*SuprAEther LLC, La Crescenta, California 91214, U.S.A*.
[2]*Sigma-1: Fabrication Manufacturing Science, Los Alamos National Laboratory, Los Alamos, NM, 87545, U.S.A*.
[3]*Jacobs Engineering, Inc., Huntsville, AL 35812, U.S.A*.
[4]*NASA Marshall Space Flight Center, Huntsville, AL 35812, U.S.A*.

The authors declare that they have no known competing financial interests or personal relationships that could have appeared to influence the work reported in this paper.